Cascaded photoenhancement: Implications for photonic chemical and biological sensors

Kirk A. Fuller
National Space Science and Technology Center, University of Alabama in Huntsville, Huntsville, AL, 35899
fuller@nsstc.uah.edu

David D. Smith
NASA-Marshall Space Flight Center, Space Transportation Directorate EV43, Huntsville, AL, 35726
david.d.smith@msfc.nasa.gov

Abstract: Our analysis shows that coupling of gold nanoparticles to microspheres will evoke a cascading effect from the respective photoenhancement mechanisms. We refer to this amplification process as cascaded photoenhancement, and the resulting cavity amplification of surface-enhanced Raman scattering (SERS) and fluorescence as CASERS and CAF, respectively. Calculations, based on modal analysis of scattering and absorption by compound spheres, presented herein indicate that the absorption cross sections of metal nanoparticles immobilized onto dielectric microspheres can be greatly enhanced by cavity resonances in the microspheres without significant degradation of the resonators. Gain factors associated with CSP of $10^3 - 10^4$ are predicted for realistic experimental conditions using homogenous microspheres. Cascaded surface photoenhancement thus has the potential of dramatically increasing the sensitivities of fluorescence and vibrational spectroscopies.

OCIS codes: (130.6010) Sensors; (140.4780) Optical resonators

References and links

1. Purcell, E. M., "Spontaneous emission probabilities at radio frequencies," Phys. Rev. **69**, 681 (1946).
2. Drexhage, K. H., *Progress in Optics*, vol. 12 (E. Wolf Ed., North-Holland, Amsterdam, 1974).
3. Lakowicz, J. R., I. Gryczynski, Y. Shen, J. Malicka, and Z. Gryczynski, "Intensified Fluorescence: Radiative decay engineering uses metal particles to enhance fluorescence, suggesting myriad new applications in biotechnology and chemistry," Photonics Spectra p. 96 (2001).
4. Lakowicz, J. R., Y. Shen, S. D'Auria, J. Malicka, J. Fang, Z. Gryczynski, and I. Gryczynski, "Radiative decay engineering," Analytical Biochem. **301**, 261 (2002).
5. Gryczynski Z., J. Malicka, I. Gryczynski, E. Matveeva, C. D. Geddes, K. Aslan, and J. R. Lakowicz, "Metal-enhanced fluorescence: A novel approach to ultra-sensitive fluorescence sensing assay platforms," in *Biomedical Vibrational Spectroscopy and Biohazard Detection Technologies*, A. Mahadevan-Jansen, M. G. Sowa, G. J. Puppels, Z. Gryczynski, T. Vo-Dinh, and J. R. Lakowicz, eds., pp. 275–282 (SPIE Press, Bellingham, WA, 2004).
6. Stuart, H. R. and D. G. Hall, "Absorption enhancement in silicon-on-insulator waveguides using metal island films," App. Phys. Lett. **69**, 2327 (1996).
7. Félidj, N., J. Aubard, G. Lévi, J. R. Krenn, A. Hohenau, G. Schider, A. Leitner, and F. R. Aussenegg, "Optimized surface-enhanced Raman on gold nanoparticle arrays," Appl. Phys. Lett. **82**, 3095–3097 (2003).
8. Nie, S. and S. R. Emory, "Probing single molecules and single nanoparticles by surface-enhanced Raman scattering," Science **275**, 1102–1106 (1997).

9. Kneipp, K., Y. Wang, H. Kneipp, L. T. Perelman, I. Itzkan, R. R. Dasari, and M. S. Feld, "Single molecule detection using surface-enhanced Raman scattering (SERS)," Phys. Rev. Lett. **78**, 1667–1670 (1997).
10. Xu, H., E. J. Bjerneld, M. Käll, and L. Börjesson, "Spectroscopy of single hemoglobin molecules by surface enhanced Raman scattering," Phys. Rev. Lett. **83**, 4357–4360 (1999).
11. Morris, M. D., *Biomedical Applications of Raman Spectroscopy*, vol. 3608 (Proc. Soc. Photo-Opt. Instrum. Eng., 1999).
12. Mahadevan-Jansen, A. and G. W. Puppels, *Biomedical Spectroscopy: Vibrational Spectroscopy and Other Novel Techniques*, vol. 3918 (Proc. Soc. Photo-Opt. Instrum. Eng., 2000).
13. Kneipp, K., H. Kneipp, V. B. Kartha, R. Manoharan, G. Deinum, I. Itzkan, R. R. Dasari, and M. S. Feld, "Detection and identification of a single DNA base molecule using surface-enhanced Raman scattering (SERS)," Phys. Rev. E **57**, R6281–R6284 (1998).
14. Gorodetsky, M. L., A. A. Savchenkov, and V. S. Ilchenko, "Ultimate Q of optical microsphere resonators," Opt. Lett. **21**, 453–455 (1996).
15. Vernooy, D. W., V. S. Ilchenko, H. Mabuchi, E. W. Streed, and H. J. Kimble, "High-Q measurements of fused-silica microspheres in the infrared," Opt. Lett. **23**, 247–249 (1998).
16. Arnold, S., J. Communale, W. B. Whitten, J. M. Ramsey, and K. A. Fuller, "Room-temperature microparticle-based persistent hole-burning memory spectroscopy," J. Opt. Soc. Am. B **9**, 4081–4093 (1992).
17. Chang, R. K. and A. J. Campillo, *Optical Processes in Microcavities* (World Scientific, Singapore, 1996).
18. Vollmer, F., D. Braun, A. Libchaber, M. Khoshsima, I. Teraoka, and S. Arnold, "Protein detection by optical shift of a resonant cavity," Appl. Phys. Lett. **80**, 4057–4059 (2002).
19. Vollmer, F., S. Arnold, D. Braun, I. Teraoka, and A. Libchaber, "Multiplexed DNA Quantification by Spectroscopic Shift of Two Microsphere Cavities," Biophys. J. **85**, 1974–1979 (2003).
20. Arnold, S., M. Khoshsima, I. Teraoka, S. Holler, and F. Vollmer, "Shift of whispering-gallery modes in microspheres by protein adsorption," Opt. Lett. **28**, 272–274 (2003).
21. Blair, S. and Y. Chen, "Resonant-enhanced evanescent-wave fluorescence biosensing with cylindrical optical cavities," Appl. Opt. **40**, 570–582 (2001).
22. Boyd, W. R. and J. E. Heebner, "Sensitive disk resonantor photonic biosensor," Appl. Opt. **40**, 5742–5747 (2001).
23. Krioukov, E., D. J. W. Klunder, A. Driessen, J. Greve, and C. Otto, "Sensor based on an integrated optical microcavity," Opt. Lett. **27**, 512–514 (2002).
24. Krioukov, E., D. J. W. Klunder, A. Driessen, J. Greve, and C. Otto, "Integrated optical microcavities for enhanced evanescent-wave spectroscopy," Opt. Lett. **27**, 1504–1506 (2002).
25. Bohren, C. F. and D. R. Huffman, *Absorption and Scattering of Light by Small Particles* (Wiley, New York, 1983).
26. Smith, D. D. and K. A. Fuller, "Photonic Bandgaps in Mie Scattering by Concentrically Stratified Spheres," J. Opt. Soc. Am. B **19**, 2449–2455 (2002).
27. Fuller, K. A. and D. W. Mackowski, "Light Scattering by Compounded Spherical Particles," in *Light Scattering by Nonspherical Particles: Theory, Measurements and Applications*, M. I. Mishchenko, J. W. Hovenier, and L. D. Travis, eds. (Academic Press, New York, 2000).
28. Fuller, K. A. and D. D. Smith, "Local intensity enhancements in spherical microcavities: implications for photonic chemical and biological sensors," in *The 2004 NASA Faculty Fellowship Program Research Reports*, J. Bland, ed. (Marshall Space Flight Center, 2005, or http://vortex.nsstc.uah.edu/amuor/nffp04.html).
29. Arnold, S., C. T. Liu, W. B. Whitten, and J. M. Ramsey, "Room-temperature microparticle based persistent spectral hole burning memory," Opt. Lett. **16**, 420–422 (1991).
30. Fuller, K. A. and D. D. Smith, "The matrix reloaded: Characteristic matrices for spherical shell photonic systems," in *The 2003 NASA Faculty Fellowship Program Research Reports*, J. Bland, ed. (Marshall Space Flight Center, 2004, or http://vortex.nsstc.uah.edu/amuor/nffp03.html).

1. Introduction

In this section, we briefly summarize the constituent enhancement mechanisms relevant to this work. In subsequent sections we review the theory upon which our calculations are based and present results of calculations for microsphere-nanoparticle cascaded surface photoenhancement mechanisms. We conclude with discussions of means for optically interrogating such systems under realistic laboratory conditions.

An important postulate of cavity quantum electrodynamics (CQED) states that the spontaneous emission properties of an atom or molecule are not independent of the surrounding electromagnetic environment, but are dependent on the density of modes in the vicinity of the emitter [1]. It has been amply demonstrated that the presence of a surface near an emitting molecule substantially increases the intensity of fluorescence emission due to an increase in

the local density of modes [2]. Similarly, metal nanoparticles and quantum dots can also lead to dramatically increased fluorescence intensities. In fact, the quantum yield of molecules that typically have almost negligible fluorescence, such as DNA, can be increased to almost unity through the introduction of metal nanoparticles, a process that has been referred to as radiative decay engineering [3]–[5]. Moreover, Stuart and Hall [6] have shown that the response of metal nanoparticles can become coupled with the modes of a nearby waveguide such that absorption or coupling between metal particles is enhanced. Taken together, those studies suggest that coupling of nanoparticles to microcavities might be employed to manipulate the density of modes in a multiplicative fashion to control emission and perhaps other inelastic processes, as well.

Raman spectra can be generated through the use of a very strong light source that stimulates inelastic light scattering by molecules, with the scattering being most prominent at wavelength shifts associated with the molecules' natural vibrational frequencies. The Raman signal can be greatly enhanced by exposing a molecule to the intense electric fields that arise near surfaces exhibiting nanoscale roughness. This is known as surface-enhanced Raman scattering (SERS). SERS typically produces gain factors of $10^3 - 10^6$, but under special conditions, factors of $10^{10} - 10^{14}$ have been achieved [7], rivaling those for fluorescence [8], and pushing detection limits back to the level of single molecules [9]. As difficulties associated with reproducible preparation of strongly enhancing surfaces have been overcome, SERS has become increasingly important in bioanalytical chemistry [7]-[13].

An intriguing mechanism for localized enhancement of energy density arises from whispering gallery modes (WGMs) that appear at sharply defined spectral positions in microcavity resonators. Within such resonators light may be trapped in circular orbits as it undergoes multiple total internal reflections (TIR) at the inner surface of the sphere. For a given diameter and refractive index a sphere will sustain a WGM if the internally reflected light returns in phase after a complete orbit. The fundamental quantity describing the power loss of a resonant structure is its quality factor or Q. This factor is defined as the ratio 2π(stored energy)/(energy lost per cycle), which for Lorentzian line shapes such as those encountered with WGMs is simply $Q = \omega_0/\Delta\omega$, where ω_0 is the resonance frequency in radians and $\Delta\omega$ is the full width at half max of the lineshape. WGMs, also known as morphology-dependent resonances (MDRs), can sustain Qs of up to 10^{10} [5] [14], [15]. The dramatic increases in photon densities within these microcavities have been shown to produce low-threshold nonlinear optical effects such as stimulated Raman scattering, lasing, spectral hole burning, and cavity quantum electrodynamic effects [16], [17].

In addition to very high photon densities in the mode volumes of microcavities, very strong evanescent fields reside on and near their outer surfaces. Vigorous research has begun into ways to use these strong surface fields to detect and analyze minute amounts of molecular species adsorbed onto the resonator. Optical shifts in MDRs have been used to detect adsorption of proteins onto glass spheroids [18]-[20], and resonant enhanced evanescent wave fluorescence has been proposed for photonic biosensing [21], as have integrated optical microcavities [22]-[24]. These latter references suggest that detection limits of 20-100 molecules are possible.

The work presented here explores how inelastic processes, such as Raman scattering and fluorescence emission, that are enhanced by the strong electric fields that arise near metal nanoparticles, may be further amplified by the strong evanescent fields of microresonators.

2. Theory

The electric and magnetic fields that arise from the interaction of microspheres with plane wave radiation may be readily expressed in terms of vector spherical harmonics $\mathbf{N}_{mnp}$. The vector spherical harmonics may be written in terms of regular (Rg) and irregular (Ig) components, viz., $\mathbf{N}_{mnp} = Rg\mathbf{N}_{mnp} + iIg\mathbf{N}_{mnp}$, as determined by the behavior of the spherical Bessel and

Hankel functions which govern their radial dependence. The subscripts mn are the azimuthal and polar mode numbers, respectively, of the harmonics and the subscript p denotes TM ($p = 1$) or TE ($p = 2$) polarization.

The expansion for the incident field, taken here to be an infinite plane wave, is

$$\mathbf{E}^{\text{inc}} = \sum_{m=\pm 1, np} q_{mnp} Rg\mathbf{N}_{mnp}. \tag{1}$$

The scattered and transmitted (internal) fields may be expressed, respectively, as

$$\mathbf{E}^{\text{sca}} = \sum_{m=\pm 1, np} q_{mnp}\, a_{np}\, \mathbf{N}_{mnp}, \tag{2}$$

$$\mathbf{E}^{\text{tra}} = \sum_{m=\pm 1, np} q_{mnp}\, c_{np}\, Rg\mathbf{N}_{mnp}, \tag{3}$$

where the expansion coefficients a_{mnp} and c_{mnp} are functions of the sphere's refractive index m, radius a, and the wavelength λ of the incident radiation. These coefficients and the expansion coefficients q_{mnp} of the incident plane wave are well-known (cf., [25] and [26]). WGMs correspond to poles in the expansion coefficients for the scattered and transmitted fields, with the sequence of poles that are encountered with decreasing wavelength giving rise to increasing orders of resonance.

The characteristic response of a resonator tuned to a WGM is displayed in Figure 1. This figure was generated from calculations of $|\mathbf{E}^{\text{sca}}|^2/|\mathbf{E}^{\text{inc}}|^2$ for a microsphere tuned to a 2nd-order resonance. (The order of the resonance can be determined by the number of concentric rings of high intensity in the mode volume of the resonator.) The plot on the right in Figure 1 was made with the internal fields set to zero in order to clearly illustrate the intensity of the evanescent fields that reside very near the surface of the cavity. When, as in this case, the resonances are stimulated by free-space coupling of a beam of light to a microspheres, counter propagating waves are set up in the mode volume and the resulting $|E|^2$ displays a standing wave pattern. If one adds the magnetic contribution $|H|^2$, the energy density will be profiled and the standing wave pattern will be much less pronounced.

In order to study CSP, one must be able to account for electrodynamic coupling between microspheres and particles (also assumed spherical) attached to them. This is accomplished with the theory for scattering and absorption by compounded spheres, which is reviewed in [27], and briefly summarized here.

In general the plane wave coefficients are given by

$$q_{mnp} = \left\langle \mathbf{N}_{mnp} \middle| \mathbf{E}^{\text{inc}} \right\rangle. \tag{4}$$

In the case of a single sphere, the mathematics may be simplified by assuming the incident beam to propagate along the z-axis of the coordinate system, in which case only the terms $m = \pm 1$ survive the integration.

On the other hand, for an ensemble of N_s spheres, azimuthal symmetry cannot be assumed and we have

$$\mathbf{E}^{\text{sca}} = \sum_{\ell=1}^{N_S} \sum_{mnp} {}^{\ell}q_{mnp}\, {}^{\ell}a_{mnp}\, \mathbf{N}_{mnp}(k\mathbf{r}_{\ell}), \tag{5}$$

where the index ℓ indicates that the origin of the vector spherical harmonics is taken to be the center of the ℓth sphere. The coefficients ${}^{\ell}a_{mnp}$ are the amplitudes of the partial waves scattered by the ℓth sphere, with all interparticle interactions accounted for.

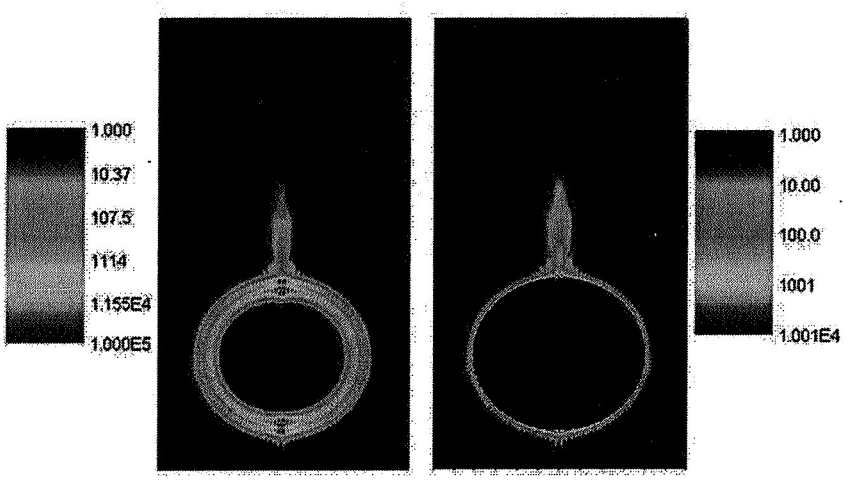

Fig. 1. Electromagnetic energy density in the equatorial plain of a microsphere tuned to a 2nd-order resonance.

Application of the addition theorem for vector spherical harmonics and of the boundary conditions imposed by Maxwell's equations allows the expansion coefficients of the scattered field of the ensemble to be written as the self-consistent set of equations

$$^{\ell}a_{mnp} = d^{\ell}_{np}\left(q^{\ell}_{mnp} + \sum_{\ell'=1}^{N_s}\sum_{jkl} A^{\ell\ell'}_{mnpjkl}\, d^{\ell'}_{jkl}\right), \quad \ell \neq \ell', . \tag{6}$$

The first term in parentheses represents partial waves of the incident field and the summation represents partial waves arriving at the ℓth sphere from scattering by all other spheres in the ensemble. Multiplying these terms is the Lorenz-Mie coefficient of the ℓth sphere. The coupling coefficients is this latter expansion are given by

$$A^{\ell\ell'}_{mnpjkl} = \langle \mathbf{N}_{mnp}(k\mathbf{r}_{\ell}) | \mathbf{N}_{jkl}(k\mathbf{r}'_{\ell}) \rangle \tag{7}$$

(Once the expansion coefficients of a multilayered sphere are known, they may be substituted for the coefficients of a homogeneous sphere and Eq. 6 solved for collections of multilayered spheres.) A more complete review of the theory for scattering and absorption by compounded spheres is provided in [27].

3. Calculations for Au nanospheres on microspherical resonators

A critical question related to the interaction between nanoparticles and microspheres is whether or not the nanoparticles could spoil the $Q$of microsphere WGMs. To consider this issue, calculations were made of the absorption cross sections C_{abs} of nanoparticles on lossless dielectric

microspheres. Figure 2 shows how the absorption efficiency Q_{abs} (= C_{abs} divided by the particle's geometric cross section) of a Au nanoparticle may be enhanced near the surface of a microcavity as the wavelength of the incident beam is tuned through a series of microsphere WGMs. There is no absorption in the microsphere itself, and so this graph shows that the Au

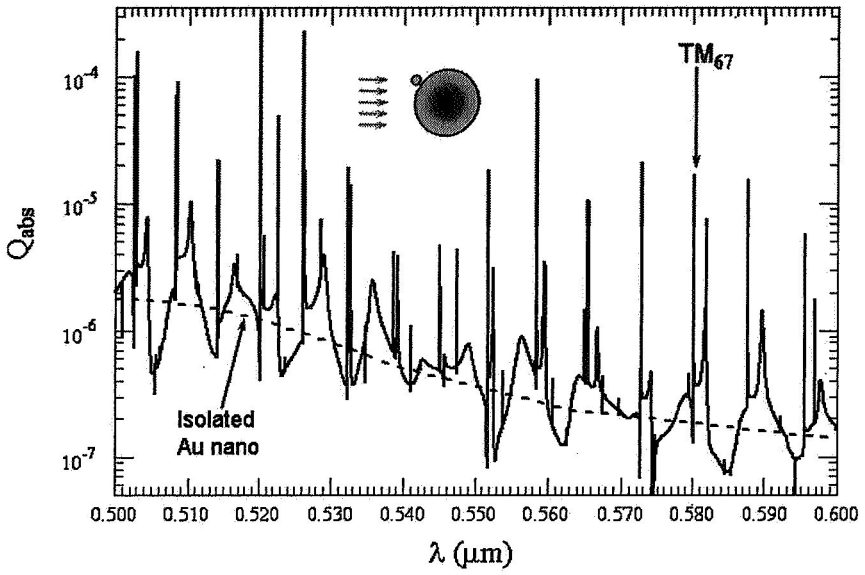

Fig. 2. Absorption efficiency spectrum of a 20 nm diameter Au sphere on a 5 μm diameter latex microbead. The position of the nanoparticle (not drawn to scale) relative to the incident beam is shown in the inset. The absorption efficiency of the nanoparticle in the absence of the sphere is given by the black curve.

nanoparticle is being exposed to greatly enhanced local intensities, but does not produce feedback significant enough to degrade the resonance. The electromagnetic 'terrain' responsible for this resonance-enhanced absorption is shown in Fig. 1.

Calculations for numerous orientations were made. In all cases, orders-of-magnitude enhancements of Q_{abs} were found for nanoparticles coupled to a microcavity relative to the case of an isolated nanoparticle.[28]

While these calculations are for a single nanoparticle, preliminary measurements of the resonance spectra of a microsphere with Au nanoparticles lightly dispersed over its surface indicate that the WGMs are sustained under such conditions, albeit with the quality factors diminished somewhat.

4. Some considerations regarding interparticle and substrate coupling

It has been shown [16] that one may observe resonance effects in populations of microbeads of sufficiently narrow size distribution to ensure that a significant fraction of spheres are tuned to the same resonance. More typically, however, the breadth of the size distribution of a collection of spheres will severely broaden WGM features of the ensemble. On the other hand, one may image individual spheres in such a collection in order to observe CASERS and CAF effects. Either case involves microspheres residing on a substrate or in contact with other microspheres, and one must consider the effects of coupling between the resonators and of coupling between the resonators and a substrate. Earlier measurements and calculations [16], [29] show that for

some geometries, these coupling effects will not have a significant effect. In these cases, the beams were angled relative to the microbead array and the substrate in such a way that coupling was minimized.

Here, we explore numerically the effects of a beam directed along the line of centers of a pair of spheres. This is the condition for strongest interparticle coupling. By increasing the size of one sphere to many times that of the other, this also allows us to approximate the condition of a sphere on a locally flat surface, provided that the 'substrate' sphere is absorbing and therefore the smaller sphere is not exposed to retroreflections from the larger one.

For the calculations used to generate Figure 3, one of the spheres was tuned to a high-Q resonance and its size held constant. With the wavelength locked to the resonance frequency of that sphere, a second sphere is introduced. The size of the second sphere varied by four orders of magnitude.

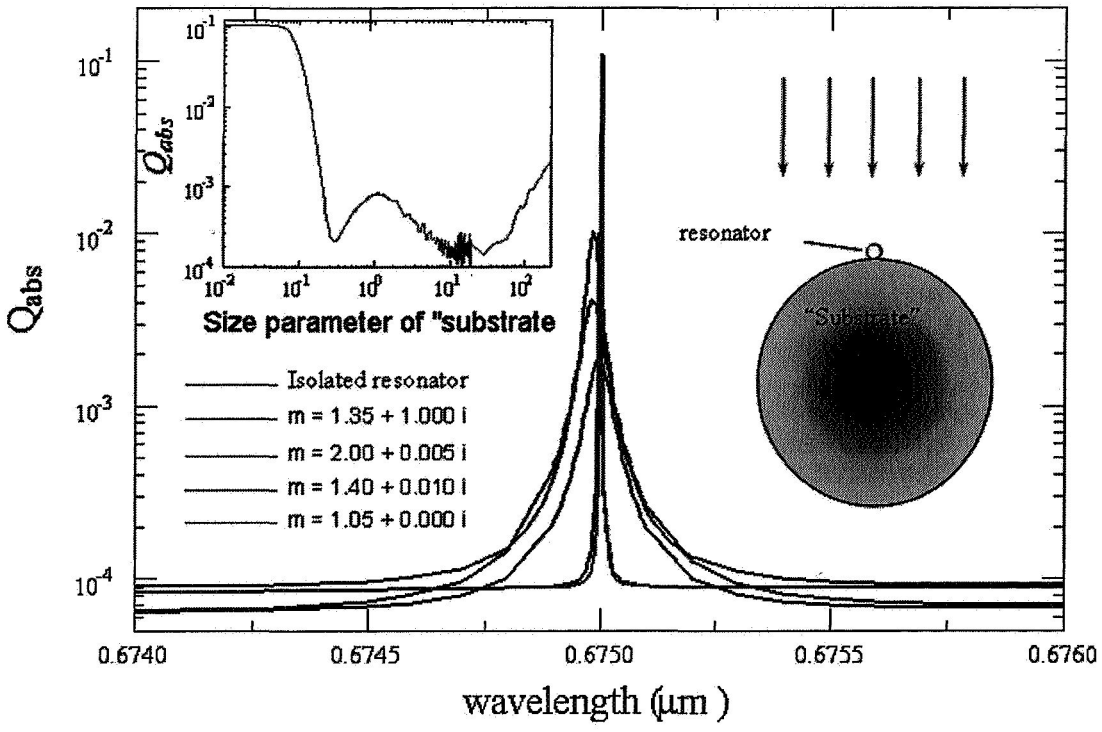

Fig. 3. Some effects of interparticle and substrate coupling on WGM resonances.

The size parameter of a sphere is defined as the ratio of its circumference to the wavelength of incident light. The size parameter of the second sphere was allowed to grow from 0.01 to a little over 200, at which point problems with machine memory were encountered. A small amount of absorption was introduced in the resonator, represented by the imaginary part of its complex index of refraction being set to $\sim 10^{-6}$. This absorption was small enough to avoid Q-spoiling and produced 3-order-of-magnitude spikes in Q_{abs} when the sphere was tuned to a resonance. Absorption in the second sphere was large enough to prevent resonance and to prevent retroreflections back onto the resonantor that would have complicated interpretation of the results as the second sphere became large.

Modal analysis allows one to readily calculate Q_{abs} for the individual spheres. The plots in

Figure 3 are for the Q_{abs} of the resonator only.

5. Discussion and conclusions

The enhancement of the intensity of Raman scattering by metal nanoparticles is expressed in terms of incident and scattered local electric field amplitudes E_{loc} as

$$I_{SERS} \propto \frac{|E_{loc}(\omega_{exc})|^2}{|E_0(\omega_{exc})|^2} \frac{|E_{loc}(\omega_{RS})|^2}{|E_0(\omega_{RS})|^2}, \tag{8}$$

where ω_{exc} and ω_{RS} are the circular frequencies of the incident (excitation) and Raman scattered light, respectively. Excitation of the nanoparticle-microsphere systems discussed above and studied in [30] results in gains of

$$|E_{loc}(\omega_{exc})|^2/|E_0(\omega_{exc})|^2 \approx 10^2 - 10^4.$$

Calculations presented here thus indicate that the absorption cross sections of metal nanoparticles or quantum dots immobilized onto dielectric microspheres can be greatly enhanced by cavity resonances in the microspheres. Molecules attached to the immobilized nanoparticles would thus experience cascaded surface-photoenhancements (CSPs), leading to additional gains in fluorescence and Raman scattering of several orders of magnitude over conventional radiative decay engineering and SERS effects. Gain factors of $10^3 - 10^4$ are predicted for realistic experimental conditions using homogenous microspheres.

For illustrative purposes, the refractive index of the microsphere used to generate Figure 2 was that of latex. For cavity amplification of SERS, one must choose microcavities that are made from materials, such as silica, that will not themselves produce a strong Raman background signal. The Q_{abs} spectra and local energy densities will be similar for equivalent resonance modes, regardless of the dielectric chosen.

Acknowledgments Rosenberger - preliminary measurements on effect of Au nanoparticle deposits on microsphere resonances.